Vertical Hole Transport and Carrier Localization in InAs/InAs_{1−x}Sb_{x} Type-II Superlattice Heterojunction Bipolar Transistors

B. V. Olson, J. F. Klem, E. A. Kadlec, J. K. Kim, M. D. Goldflam, S. D. Hawkins, A. Tauke-Pedretti, W. T. Coon, T. R. Fortune, E. A. Shaner, and M. E. Flatté

Phys. Rev. Applied **7**, 024016 — Published 13 February 2017

DOI: 10.1103/PhysRevApplied.7.024016

Vertical hole transport and carrier localization in $InAs/InAs_{1-x}Sb_x$ type-II superlattices heterojunction bipolar transistors

B. V. Olson,* J. F. Klem, E. A. Kadlec, J. K. Kim, M. D. Goldflam,
S. D. Hawkins, A. Tauke-Pedretti, W. T. Coon, T. R. Fortune, and E. A. Shaner†
Sandia National Laboratories, Albuquerque, New Mexico 87185, USA

M. E. Flatté
Department of Physics and Astronomy and Optical Science and Technology Center, University of Iowa, Iowa City, IA 52242, USA

(Dated: January 17, 2017)

Abstract

Heterojunction bipolar transistors are used to measure vertical hole transport in narrow-bandgap $InAs/InAs_{1-x}Sb_x$ type-II superlattices (T2SLs). Vertical hole mobilities (μ_h) are reported and found to decrease rapidly from 360 cm^2/V-s at 120 K to $\approx$2 cm^2/V-s at 30 K, providing evidence that holes are confined to localized states near the T2SL valence miniband edge at low temperatures. Four distinct transport regimes are identified: (1) pure miniband transport, (2) miniband transport degraded by temporary capture of holes in localized states, (3) hopping transport between localized states in a mobility edge, and (4) hopping transport through defect states near the T2SL valence miniband edge. Region (2) is found to have a thermal activation energy of $\varepsilon_2 = 36$ meV, corresponding to the energy range of a mobility edge. Region (3) is found to have a thermal activation energy of $\varepsilon_3 = 16$ meV, corresponding to the hopping transport activation energy. This description of vertical hole transport is analogous to electronic transport observed in disordered amorphous semiconductors displaying Anderson localization. For the T2SL, we postulate that localized states are created by disorder in the group-V alloy of the $InAs_{1-x}Sb_x$ hole well causing fluctuations in the T2SL valence band energy.

* Current address: Vixar Inc., 2950 Xenium Ave Lane N., Plymouth, MN 55441; Email: bolson@vixarinc.com

† Email: eashane@sandia.gov

I. INTRODUCTION

Charge carrier drift and diffusion in superlattices (SLs) is significantly different from bulk charge transport due to the presence of the periodic potential wells along the growth axis [1, 2]. In-plane transport, defined as transport parallel to the SL growth layers, can be reminiscent of bulk transport in magnitude, but the limiting scattering mechanisms are typically quite different [3]. Efficient vertical, otherwise known as perpendicular, transport in a SL, however, relies on the transport through extended Bloch states along the SL growth direction [4], which have strict criteria in order to exist [5]. This directionality in relation to the SL layers is defined by the axes in Fig. 1(b). While SL in-plane transport can be readily interrogated using Hall measurements [3], SL vertical transport remains a challenge to measure. Direct measurements are typically reliant on ultrafast all-optical time-of-flight experiments with structures engineered to capture diffusing charge carriers [1, 2, 6–9] or electron beam induced microscopy measurements [10].

In this *Letter*, vertical minority carrier hole transport in infrared (IR) InAs/$InAs_{1-x}Sb_x$ type-II superlattices (T2SLs) is measured using band-engineered heterojunction bipolar transistor (HBT) devices, providing a simpler approach to measuring critical vertical transport properties. Heterojunction bipolar transistors are quintessential minority carrier transport devices [11] and provide an ideal platform with which to study fundamental transport properties in these narrow-bandgap T2SL structures. InAs/$InAs_{1-x}Sb_x$ T2SLs are themselves of considerable interest for next-generation IR photodetectors due to their realization of long minority carrier lifetimes (τ_{MC}) [12–14].

However, little is known about the fundamental transport behavior along the growth direction in InAs/$InAs_{1-x}Sb_x$ T2SLs. Additionally, current state-of-the-art photodetector architectures utilize a *nBn* design [15], which use holes as the carriers of the photocurrent. Vertical hole transport is therefore critical to measure in this material system. While vertical transport in *n*-type InAs/$InAs_{1-x}Sb_x$ T2SLs has been previously measured [10], no clear picture of how the vertical hole transport proceeds in this material is yet available. Here, both electrical and optical measurements on T2SL HBT devices are used to characterize the vertical hole mobility over a range of temperatures. The experimental results indicate that carrier localization [2] plays an important role in the vertical hole transport and suggest the presence of a mobility edge and defect level through which hopping transport occurs, analo-

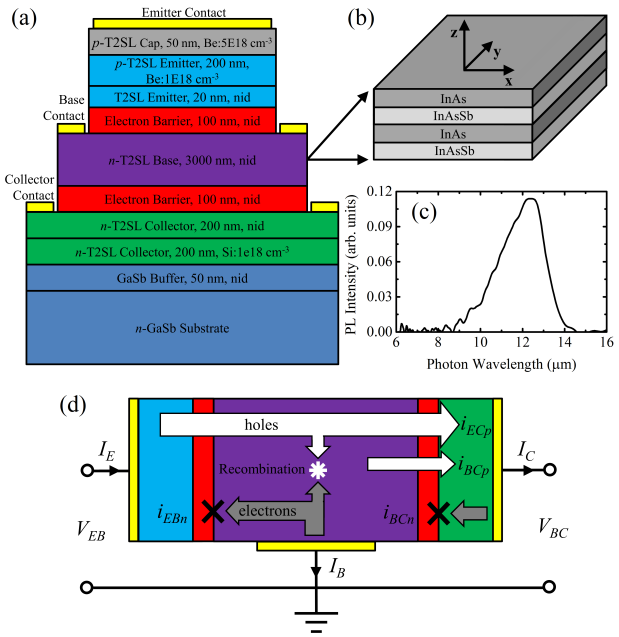

FIG. 1. (a) Schematic of the type-II superlattice (T2SL) heterojunction bipolar transistor (HBT) epitaxial growth structure. (b) Zoomed view of the T2SL layers with the axes defining the transport directions: $\mathbf{x}, \mathbf{y}$ are the in-plane directions and $\mathbf{z}$ is the vertical direction. (c) 18 K photoluminescence from the HBT structures demonstrating the long-wave infrared bandgap energy of the T2SL layers. (d) Electrical schematic of the T2SL HBT device in the common-base configuration with the various currents identified.

gous to electronic transport in amorphous semiconductors displaying Anderson localization [16].

II. SAMPLE AND METHODS

The HBT devices are grown by molecular beam epitaxy (MBE) on a tellurium-doped n-type GaSb substrate with a (100) orientation. Fig. 1(a)-(b) show the epitaxial growth stack. The T2SL layers, entailing the emitter, base, and collector regions, all consist of a repeating sequence of 102.6 Å $InAs_{0.97}Sb_{0.03}$/18.9 Å $InAs_{0.55}Sb_{0.45}$. The slight residual Sb content in the InAs layer is due to Sb cross-incorporation from the alloy layers into the InAs layers during growth [17]. Equilibrium majority electron concentrations of approximately $0.5-1.0\times10^{15}$ cm^{-3} are typical in not intentionally doped (*nid*) n-type T2SL layers from this MBE reactor. Low temperature photoluminescence (PL) spectra, shown in Fig. 1(c), of the

HBT structures exhibit strong IR emission with a peak wavelength of 12.5 μm, consistent with the predicted bandgap for this T2SL structure [18].

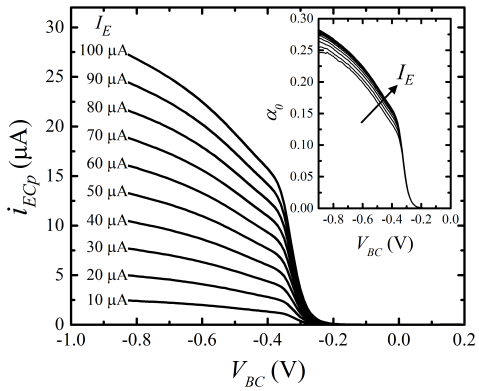

FIG. 2. Dependence that the injected heavy hole diffusion component of I_C has on the base-collector voltage at 60 K. Individual curves are for different constant emitter currents. The inset shows the 60 K common base current gain for the same emitter currents.

Under operation, the emitter-base junction is forward biased to inject holes into the n-type T2SL base region. These holes either diffuse across the base region to the base-collector junction and make up the emitter hole diffusion component (i_{ECp}) of the total collector current (I_C), or recombine in the base. Wide bandgap layers integrated into the HBT junctions are engineered to block the flow of parasitic electron currents, shown in Fig. 1(d), while allowing hole currents to flow unimpeded. The component of I_C related to injected holes diffusing across the thick T2SL base region is thus $i_{ECp} = I_C - i_{BCp}$, where i_{BCp} is the hole current arising from charge generation in the base.

The hole diffusion current is shown in Fig. 2 at a temperature of 60 K for different emitter currents. Collection of diffusing holes begins at $V_{BC} \approx -0.25$ V and requires $V_{BC} \approx -0.4$ V to reach saturation. For larger reverse biases, i_{ECp} monotonically increases. This effect is attributed to narrowing of the *nid* T2SL base region at large V_{BC} [11], which has been confirmed by capacitance-voltage (C-V) measurements. Both the emitter and collector contacts have thin stand-off regions to ensure depletion of the *nid* T2SL base region is minimal at small biases. The C-V measurements confirm that the T2SL base region remains relatively undepleted at $V_{BC} = -0.4$ V such that the hole transport distance can be set equal to the base thickness of 3 μm.

III. EXPERIMENTAL RESULTS

The fraction of injected holes able to diffuse across the T2SL base region and be collected is the common base current gain (α_0), expressed as [11],

$$\alpha_0 = \frac{i_{ECp}}{I_E} = \frac{I_C - i_{BCp}}{I_E}. \tag{1}$$

The inset to Fig. 2 shows α_0 for the 60 K data. The vertical hole diffusion length (L_d) is readily determined from α_0 using [11],

$$\alpha_0 = \frac{1}{\cosh(W/L_d)}, \tag{2}$$

where W is the undepleted base thickness of 3 μm. The diffusion length of interest is taken at $V_{BC} = -0.4$ V, the base-collector voltage at which i_{ECp} is fully collected. We have assumed that the emitter efficiency for these HBT devices is approximately 1. For the 60 K data shown $L_d = 1.16$ μm.

The temperature dependence of α_0 is shown in Fig. 3. For clarity of viewing, not all temperatures have been plotted. For all temperatures measured, though, a similar bias of $V_{BC} = -0.4$ V is required to fully extract i_{ECp}. A steady decrease in the magnitude of α_0, regardless of V_{BC}, as the temperature decreases is also observed. Ultimately, for temperatures below 40 K, only a small fraction of the injected holes are able to diffuse across the T2SL base region before recombining.

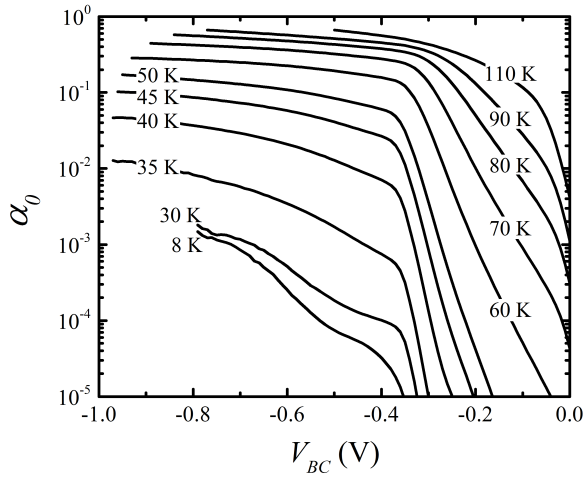

FIG. 3. Temperature dependence of the common base current gain.

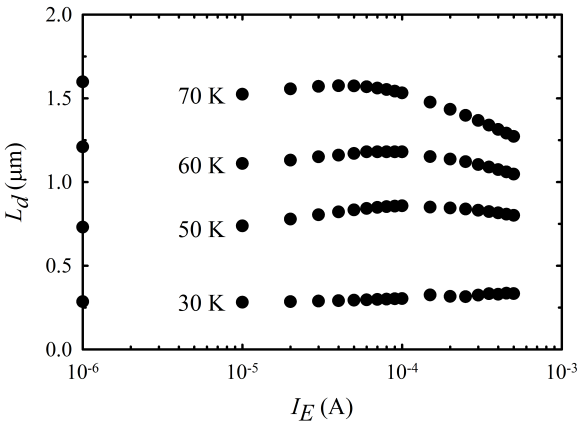

FIG. 4. Heavy hole diffusion length as a function of emitter current at three different temperatures.

The dependence that the vertical hole diffusion length has with I_E is shown in Fig. 4. Low temperatures are shown as, due to the low vertical diffusivity, ensuring minority carrier injection is suspected to be more challenging. The diffusion lengths are observed to level off to a relatively constant value as the emitter current is decreased, approaching near constant values for I_E less than a few 10^{-5} A. This indicates that the heavy hole concentration in the narrow-bandgap T2SL base region is approaching a low injection, or minority carrier transport/recombination, regime [12]. Additional measurements and modeling are necessary to confirm low injection at these currents, to fully understand the observed structure in the data at higher injection levels, and to potentially extract more information from the material.

Fig. 5 shows the resulting temperature dependence of L_d, which explicitly displays the degradation of the vertical hole transport and also that L_d becomes relatively independent of the temperature below 35 K. The peak observed in L_d at 110 K is hypothesized to be caused by more common scattering mechanisms limiting the vertical hole transport and will be discussed in a later section.

Also shown in Fig. 5 are τ_{MC} in the T2SL base region, measured using time-resolved microwave reflectance on the HBT samples [12, 18]. Interestingly, while L_d decreases from 2.55 μm to 0.28 μm from 110 K to 20 K, τ_{MC} increases from 20 ns to 227 ns over the same temperature range. Since the vertical hole diffusion coefficient (D_h) in this case is equal to L_d^2/τ_{MC} [19, 20], these opposite trends amplify the degradation to the vertical hole transport. In fact, D_h drops by three orders-of-magnitude over a 90 K temperature range, decreasing from 3.28 cm^2/s at 110 K to 0.0036 cm^2/s at 20 K.

In Fig. 6, vertical hole mobilities (μ_h) are shown, determined using Einsteins Relation

$\mu_h = (qD_h)/(k_BT)$, where q is the electronic charge, k_B is Boltzmanns constant, and T is the temperature [19]. From Fig. 4, we can assume that nondegenerate conditions apply and Einstein's Relation in the form stated is valid. A rapid decrease in μ_h from 360 cm^2/V-s at 120 K to $\approx$2 cm^2/V-s at 30 K is observed. Four distinct temperature regions are also identified, labeled (1)-(4) in Fig. 6. Regions (2) and (3) each display thermal activation-like behavior, while region (4) is relatively constant with temperature. Transitions between these different regions occur at $T_1 = 110$ K, $T_2 = 67$ K and $T_3 = 33$ K.

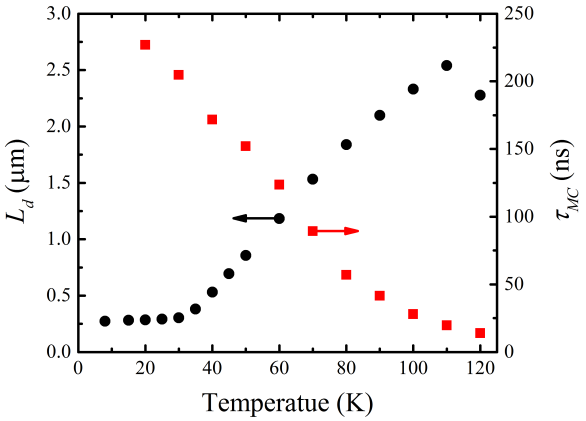

FIG. 5. Temperature dependence of the vertical heavy hole diffusion length and minority carrier lifetime in the narrow-bandgap n-type T2SL base region of the HBT devices.

IV. DISCUSSION

The mobility temperature trend is similar to electronic transport in amorphous silicon [21] and vertical charge transport in disordered SLs [2]. The vertical hole transport is interpreted in the following manner. At temperatures greater than $T_1 = 110$ K, corresponding to region (1), vertical hole transport occurs through extended Bloch states that make up the SL heavy hole miniband. The mobilities measured at 120 K and 110 K are 360 cm^2/V-s and 345 cm^2/V-s, respectively, where the 120 K mobility deviates notably from the slope in region (2). We hypothesize that this deviation is due to a more typical scattering mechanism, such as acoustic phonon scattering (μ_{AS}) which scales as $T^{-3/2}$ [22], beginning to limit μ_h.

The hole scattering time (τ_h) is related to μ_h by,

$$\mu_h = \frac{q}{m_h}\tau_h, \tag{3}$$

where m_h is the heavy hole effective mass along vertical direction, calculated from the T2SL electronic band structure [18] as $m_h = 186m_0$, where m_0 being the free electron mass. Using Eq. 3, a scattering time of 38 ps is found at 120 K. For extended Bloch states to be supported the following condition must also be met [5],

$$\frac{\Delta d}{\hbar}\tau_h > d, \tag{4}$$

where Δ is the SL heavy hole miniband width and d is the SL period thickness. This equation states that the mean free path length for, in this case, holes must be greater than d in order for transport to occur through extended Bloch states [5]. When this condition is not met, the holes become localized [5]. Using Eq. 4, the mean free path length for holes is at least 140 nm at 120 K, using a miniband width of 0.2 meV calculated from the dispersion of the heavy hole band in the electronic band structure [18], which is significantly longer than the SL period thickness of 12.09 nm. Transport of holes purely through extended Bloch states is therefore likely at temperatures greater than 110 K, supporting the relatively large μ_h measured at these temperatures.

Ionized impurity scattering (μ_{IS}), a common scattering mechanism which scales as $T^{3/2}$ [22], was initially thought to account for the measured temperature dependence of μ_h. However, as shown by the generalized curve for μ_{IS} in Fig. 6, this scattering mechanism cannot account for the drastic temperature dependence observed in μ_h. We instead attribute the temperature trend in region (2) to the thermal energy being small enough that holes interact with localized states near the T2SL valence miniband edge (E_v) created by disorder in the SL structure. In region (2), μ_h is a trap-controlled mobility with holes becoming immobilized in localized states for short periods of time. This type of transport has the form $\mu \propto e^{(E-E_v)/k_BT}$, where $\varepsilon_2 = E - E_v$ is the energy range of the localized states [23]. A fit of this form to region (2) provides an activation energy $\varepsilon_2 = 36$ meV and, as depicted in the inset to Fig. 6, corresponds to a mobility edge that extends into the T2SL bandgap.

As the temperature decreases further, holes become trapped in the localized states for longer periods of time. Eventually, for temperatures within region (3), the mean free path length for holes becomes less than d and they are fully localized. The transition between these two regions is noted by the shift in the slope of μ_h occurring at T_2 and corresponding change in activation energy from ε_2 to $\varepsilon_3 = 16$ meV. A similar transition is observed in amorphous silicon [21]. Vertical hole transport in region (3) occurs instead via phonon-

assisted hopping transport between adjacent localized states [1, 2, 9, 24–26]. In this case, ε_3 is the hopping activation energy [21, 23]. The assertion that the holes are fully localized in region (3) is supported by the condition imposed by Eq. 4, which predicts that transport through extended Bloch states will no longer occur for a hole scattering time of 3.3 ps, corresponding to a critical mobility of $\mu_h \approx 26$ cm^2/V-s. This deduced mobility at the transition from trap-controlled miniband transport to hopping transport agrees well with the mobility found at T_2.

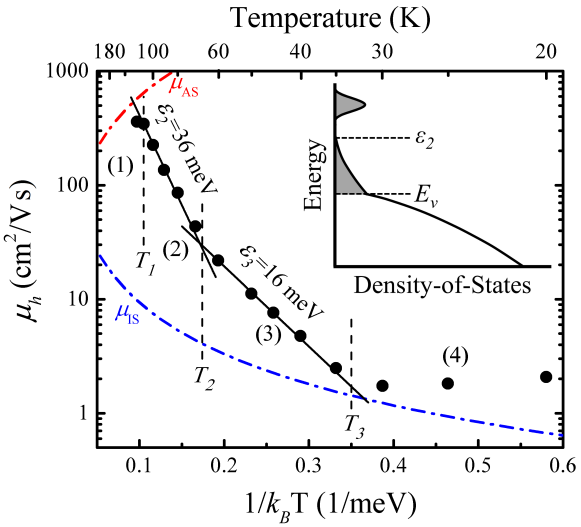

FIG. 6. Vertical hole mobilities (filled circles) measured in the narrow-bandgap type-II superlattice (T2SL). Four distinct regions are identified, separated by transition temperatures T_1, T_2, and T_3. Regions (2) and (3) are labeled with their respective activation energies. The blue and red dashed-dotted curves correspond to generalized temperature trends of ionized impurity ($\mu_{IS} \propto T^{3/2}$) and acoustic phonon ($\mu_{AS} \propto T^{-3/2}$) scattering, respectively, scaled arbitrarily. The inset illustrates the hypothesized energy range of the available states, where gray regions correspond to localized states. The activation energy ε_2 corresponds to a mobility edge extending above the T2SL valence band edge (E_v). The defect level depicted at energies above ε_2 corresponds to the hopping mobilities in region (4).

At T_3, μ_h again deviates from the behavior of the previous region and becomes relatively constant with temperature. We speculate that in region (4), the vertical hole transport occurs via hopping between defect states in a defect level near the T2SL valence miniband edge [8]. According to Mott and Davis, this type of transport should indeed have a weak

temperature dependence [23]. However, with the limited data in region (4) we cannot make any further assertions to the character of transport in this temperature range. What is certain, though, is that vertical hole transport is severely impeded at temperatures less than T_3.

It has been recently hypothesized that monolayer-type fluctuations in the SL layer thicknesses are strong enough to induce localization in InAs/$InAs_{1-x}Sb_x$ T2SLs [27]. We note that both interlayer and intralayer thickness fluctuations, and phonon scattering [5], could all potentially induce carrier localization. The effect of donor atoms themselves have also been predicted to destroy hole transport in narrow-bandgap T2SLs [28]. A recent microscopy study by Wood *et al.* on InAs/$InAs_{1-x}Sb_x$ T2SLs also showed significant disorder due to Sb segregation.

A likely source for the hole localization observed here is from fluctuations in T2SL valence band energy associated with disorder in the group-V alloy in the $InAs_{1-x}Sb_x$ hole well. A wave packet associated with a hole at 30 K would have an approximate size L of order $L = \sqrt{\hbar^2/(2m^* k_B T)}$, corresponding to $L \approx 6$ nm. The number of group-V atoms in a volume of this size is $\approx 10^4$, corresponding to a statistical fluctuation in that number of approximately 1%. The variation in E_v associated with 1% change in group-V alloy composition can be estimated from the alloy band offsets and is $\approx 2\times10^1$ meV in this case, which is reasonable considering $InAs_{1-x}Sb_x$ has large band bowing parameters [29]. Larger fluctuations may be seen at higher temperatures or if clustering is evident within the group-V alloy, which also seems likely [17]. For our purposes, this estimate suggests that the localization energies ε_2 and ε_3 are plausible.

V. CONCLUSION

Heterojunction bipolar transistor devices consisting of narrow-bandgap InAs/$InAs_{1-x}Sb_x$ T2SL emitter, base, and collector regions are used to measure vertical hole transport in the T2SL base region. In order to elucidate fundamental transport physics, the diffusion measurements are combined with optical measurements of minority carrier lifetimes in the same devices to determine the vertical hole mobilities. Four distinct regions to the vertical hole transport are identified and are explained as an effect of the holes becoming increasingly trapped in localized states near the T2SL valence band edge. At low temperatures, hopping

transport is the dominant transport mechanism. We hypothesize that disorder in the T2SL structure, caused by disorder in the group-V alloy in the $InAs_{1-x}Sb_x$ hole well, leads to a great enough fluctuation of the T2SL valence band energy to induce the observed localization. The similarities between vertical hole transport reported in this *Letter* for narrow-bandgap $InAs/InAs_{1-x}Sb_x$ T2SLs and electronic transport observed in amorphous semiconductors and other disordered SLs is striking, suggesting that disorder in the $InAs/InAs_{1-x}Sb_x$ T2SL structure has a profound impact on vertical hole transport in this emerging IR material system.

ACKNOWLEDGMENTS

Sandia National Laboratories is a multi-program laboratory managed and operated by Sandia Corporation, a wholly owned subsidiary of Lockheed Martin Corporation, for the U.S. Department of Energy's National Nuclear Security Administration under contract DE-AC04-94AL85000. This work was supported by the U.S. Department of Energy, Office of Science, Basic Energy Sciences, Materials Sciences and Engineering Division.

---

[1] B. Deveaud, J. Shah, T. C. Damen, B. Lambert, and A. Regreny. Bloch transport of electrons and holes in superlattice minibands: direct measurement by subpicosecond luminescence spectroscopy. *Phys. Rev. Lett.*, **58**, 2582 (1987).

[2] A. Chomette, B. Deveaud, A. Regreny, and G. Bastard. Observation of carrier localization in intentionally disordered GaAs/GaAlAs superlattices. *Phys. Rev. Lett.*, **57**, 1464 (1986).

[3] F. Szmulowicz, S. Elhamri, H. J. Haugan, G. J. Brown, and W. C. Mitchel. Demonstration of interface-scattering-limited electron mobilities in InAs/GaSb superlattices. *J. Appl. Phys.*, **101**, 043706 (2007).

[4] L. Esaki and R. Tsu. Superlattice and negative differential conductivity in semiconductors. *IBM J. Res. Develop.*, **14**, 61 (1970).

[5] F. Capasso, K. Mohammed, and A. Y. Cho. Resonant tunneling through double barriers, perpendicular quantum transport phenomena in superlattices, and their device applications. *IEEE J. Quant. Electron.*, **QE-22**, 1853–1869 (1986).

[6] G. D. Gilliland, A. Antonelli, D. J. Wolford, K. K. Bajaj, J. Klem, and J. A. Bradley. Direct measurement of heavy-hole exciton transport in type-II GaAs/AlAs superlattices. *Phys. Rev. Lett.*, **71**, 3717 (1993).

[7] B. Deveaud, J. Shah, T. C. Damen, B. Lambert, A. Chomette, and A. Regreny. Optical studies of perpendicular transport in semiconductor superlattices. *IEEE J. Quant. Electron.*, **24**, 1641–1651 (1988).

[8] F. Piazza, L. Pavesi, A. Vinattieri, J. Martinez-Pastor, and M. Colocci. Influence of mini-band widths and interface disorder on vertical transport in superlattices. *Phys. Rev. B*, **47**, 10625 (1993).

[9] B. V. Olson, L. M. Murray, J. P. Prineas, M. E. Flatté, J. T. Olesberg, and T. F. Boggess. All-optical measurement of vertical charge carrier transport in mid-wave infrared InAs/GaSb type-II superlattices. *Appl. Phys. Lett.*, **102**, 202101 (2013).

[10] D. Zuo, R. Liu, D. Wasserman, J. Mabon, Z.-Y. He, S. Liu, Y.-H. Zhang, E. A. Kadlec, B. V. Olson, and E. A. Shaner. Direct minority carrier transport characterization of InAs/InAsSb superlattice nBn photodetectors. *Appl. Phys. Lett.*, **106**, 071107 (2015).

[11] S. Sze and K. K. Ng. *Physics of Semiconductor Devices, 3rd Ed.* chapter 5, John Wiley and Sons, Inc., Hoboken, New Jersey (2007).

[12] B. V. Olson, E. A. Kadlec, J. K. Kim, J. F. Klem, S. D. Hawkins, M. E. Flatté, and E. A. Shaner. Intensity- and temperature-dependent carrier recombination in InAs/$InAs_{1-x}Sb_x$ type-II superlattices. *Phys. Rev. Appl.*, **3**, 044010 (2015).

[13] Y. Aytac, B. .V. Olson, J. K. Kim, E. A. Shaner, S. D. Hawkins, J. F. Klem, M. E. Flatté, and T. F. Boggess. Evidence of a Shockley-Read-Hall defect state independent of band-edge energy in InAs/In(As,Sb) type-II superlattices. *Phys. Rev. Applied*, **5**, 054016 (2016).

[14] B. V. Olson, E. A. Shaner, J. K. Kim, J. F. Klem, S. D. Hawkins, L. M. Murray, J. P. Prineas, M. E. Flatté, and T. F. Boggess. Time-resolved optical measurements of minority carrier recombination in a mid-wave infrared InAsSb alloy and InAs/InAsSb superlattice. *Appl. Phys. Lett.*, **101**, 092109 (2012).

[15] S. Maimon and G. W. Wicks. nBn detector, an infrared detector with reduced dark current and higher operating temperature. *Appl. Phys. Lett.*, **89**, 151109 (2006).

[16] P. W. Anderson. Model for the electronic structure of amorphous semiconductors. *Phys. Rev. Lett.*, **34**, 953 (1975).

[17] M. R. Wood, K. Kanedy, F. Lopez, M. Weimer, J. F. Klem, S. D. Hawkins, E. A. Shaner, and J. K. Kim. Monolayer-by-monolayer compositional analysis of InAs/InAsSb superlattices with cross-sectional STM *J. Crystal Growth*, **425**, 110–114 (2015).

[18] B. V. Olson, C. H. Grein, J. K. Kim, E. A. Kadlec, J. F. Klem, S. D. Hawkins, and E. A. Shaner. Auger recombination in long-wave infrared InAs/$InAs_{1-x}Sb_x$ type-II superlattices. *Appl. Phys. Lett.*, **107**, 261104 (2015).

[19] N. W. Ashcroft and N. Mermin. *Solid State Physics*. chapter 29, Suanders (1976).

[20] K. Weiser. Proposal for measuring anisotropic diffusivity of minority carriers in semiconductor layer structures by means of photoluminescence experiments under interference conditions. *Superlattices and Microstruct.*, **23**, 575–579 (1998).

[21] P. G. Le Comber and W. E. Spear. Electronic transport in amorphous silicon films. *Phys. Rev. Lett.*, **25**, 509 (1970).

[22] P. Y. Yu and M. Cardona. *Fundamentals of Semiconductors: Physics and Material Properties*. Springer, Heidelberg, NY, third ed. (2005).

[23] N. F. Mott and E. A. Davis. *Electronic Processes in Non-Crystalline Materials*. Oxford University Press, Inc., New York, second ed. (1979).

[24] J. F. Palmier, H. L. Person, C. Minot, A. Chomette, A. Regreny, and D. Calecki. Hopping mobility in semiconductor superlattices. *Superlattices and Microstruct.*, **1**, 67–72 (1985).

[25] L. Pavesi, E. Tuncel, B. Zimmermann, and F. K. Reinhart. Photoluminescence of disorder-induced localized states in GaAs/AlGaAs superlattices. *Phys. Rev. B*, **39**, 7788 (1989).

[26] R. G. Roberts, W. E. Hagston, P. Chen, J. E. Nicholls, and M. O'Neil. Anderson localization and Monte Carlo simulation of vertical transport in disordered finite superlattices. *J. Appl. Phys.*, **82**, 4378 (1997).

[27] Z.-Y. Lin, S. Liu, E. H. Steenbergen, and Y.-H. Zhang. Influence of carrier localization on minority carrier lifetime in InAs/InAsSb type-II suplerlattices. *Appl. Phys. Lett.*, **107**, 201107 (2015).

[28] M. Flatté and C. Pryor. Defect states in type-II strained-layer superlattices. *Proc. of SPIE*, **7608**, 760824–1 (2010).

[29] Y. Lin, D. Wang, D. Donetsky, L. Shterengas, G. Kipshidze, G. Belenky, S. P. Svensson, W. L. Sarney, and H. S. Hier. Conduction- and valence-band energies in bulk $InAs_{1-x}Sb_x$ and type-II $InAs_{1-x}Sb_x$/InAs strained-layer superlattices. *J. Electron. Mat.*, **42**, 918–926 (2013).